# A general study of actinyl hydration by molecular dynamics simulations using *ab initio* force fields

Sergio Pérez-Conesa 🆔, Francisco Torrico, José M. Martínez 🆔, Rafael R. Pappalardo 🆔, and Enrique Sánchez Marcos 🆔

View Online      Export Citation      CrossMark

## ARTICLES YOU MAY BE INTERESTED IN

Lock-in Amplifiers up to 600 MHz

Watch

# A general study of actinyl hydration by molecular dynamics simulations using *ab initio* force fields

Sergio Pérez-Conesa, [iD] Francisco Torrico, José M. Martínez, [iD] Rafael R. Pappalardo, [iD] and Enrique Sánchez Marcos[a) [iD]

## AFFILIATIONS

Departamento de Química Física, Universidad de Sevilla, 41012 Sevilla, Spain

[a)]Electronic mail: sanchez@us.es

## ABSTRACT

A set of new *ab initio* force fields for aqueous $[AnO_2]^{2+/+}$ (An = Np(VI,V), Pu(VI), Am(VI)) has been developed using the Hydrated Ion (HI) model methodology previously used for $[UO_2]^{2+}$. Except for the non-electrostatic contribution of the HI-bulk water interaction, the interaction potentials are individually parameterized. Translational diffusion coefficients, hydration enthalpies, and vibrational normal mode frequencies were calculated from the MD simulations. Physico-chemical properties satisfactorily agree with experiments validating the robustness of the force field strategy. The solvation dynamics and structure for all hexavalent actinoids are extremely similar and resemble our previous analysis of the uranyl cation. This supports the idea of using the uranyl cation as a reference for the study of other minor actinyls. The comparison between the $NpO_2^{2+}$ and $NpO_2^+$ hydration only provides significant differences in first and second shell distances and second-shell mean residence times. We propose a single general view of the $[AnO_2]^{2+/+}$ hydration structure: aqueous actinyls are amphiphilic anisotropic solutes which are equatorially conventional spherically symmetric cations capped at the poles by clathrate-like water structures.

*Published under license by AIP Publishing.* https://doi.org/10.1063/1.5083216

## I. INTRODUCTION

The solution chemistry of actinoid cations is a challenging yet important technological and environmental issue. Nuclear technology draws knowledge from many fields: physics, chemistry, environmental science, engineering, etc.[1] Actinyl aqua ion $[AnO_2(H_2O)_m]^{q+}$ chemistry is very important in spent nuclear fuel reprocessing and storage.[2–8] For instance, U and Pu are under their actinyl form in the PUREX method which is a liquid-liquid extraction process used to separate U and Pu from minor actinoids in dissolved nuclear fuel.[9] Their diffusion, redox, acid-base and solubility properties determine their speciation and presence in natural systems as well as their risk management in permanent geological facilities.

Actinyls are *trans*-dioxo molecular cations with chemical formula $[AnO_2]^{2+/+}$, the actinide atom being in a pentavalent or hexavalent oxidation state. The elements that form stable actinyls are uranium, neptunium, plutonium, and americium.[10] For Am, the

most stable form is its Am(III) aquaion, but Am(V,VI) also exist and are relatively stable, in highly acidic and oxidizing media.[11] The most stable species for Np is $[NpO_2]^+$, but $[NpO_2]^{2+}$ has also been reported.[10] Plutonium can be found in oxidation states from III to VI, being the Pu(IV) aquaion the most stable although the Pu(VI) actinyl form is also technologically and environmentally important.[12] In this work, we focus on U(VI), Pu(VI), Np(VI), and Am(VI) but as well as on Np(V) for comparison with a singly charged actinyl cation. The aqueous coordination chemistry of these species in acid media is very similar for all of them and are mainly pentahydrated ions, $[AnO_2·(H_2O)_5]^{2+/+}$.

Statistical simulation of aqueous uranyl has a long and successful history.[13–21] By contrast, there are only two studies that extend the computational study of uranyl to other elements. Odoh *et al.*[22] carried out Car-Parrinello Molecular Dynamics[23] (CPMD) on aqueous $[PuO_2]^{2+/+}$ studying the relative stability of different coordination numbers and hydrolysis. The only force field for actinyls beyond uranium is the one developed by the Maginn group[24] in

which they extend their previous uranyl model.[17] They developed Lennard-Jones parameters for a general $[AnO_2]^{2+/+}$(aq) system, and the partial charges and bonding terms of the molecular cation specify the element and oxidation state.

The most common force field model of an ion in solution is to consider the ion as a charged particle with Lennard-Jones parameters that are combined with those of the solvent (a "charged soft sphere model"). This model benefits from being very simple and easy to transfer to new systems applying combination rules without further parameterization. But its accuracy is limited especially for highly charged or polarizing cations. It neglects charge transfer and polarization effects suffered by first-shell solvent molecules. Therefore, it treats first-shell-bulk water molecule interactions as regular bulk water molecule interactions.

In the 1990s, our group proposed a strategy to parameterize *ab initio* interaction potentials for highly charged metal ions based on the old electrochemistry concept of the *Hydrated Ion* (HI).[25–28] Its key idea is that highly charged metal cations ($M^{q+}$) are better represented in solution by their hydrated form $[M(H_2O)_m]^{q+}$.[29] HI models for a diverse set of ions have been developed providing a reasonable description of the energetic, structural, spectroscopical, and dynamic properties of cations forming well defined aqua ions in water.[28,30–32] The recent development of the $[UO_2 \cdot (H_2O)_5]^{2+}$-$H_2O$ force field[21] was the first time that the HI model was applied to a molecular cation. The derived MD simulations provided some interesting insights into its solvation structure and dynamics.[21] Considering the similar chemical nature of An(v,vi), it is easy to anticipate that most of the methodology and knowledge of the previous U(vi) system could be transferred to broaden our knowledge of actinyl cations as done in the past with monoatomic cations of more dissimilar nature such as $Be^{2+}$, $Mg^{2+}$, $Ir^{3+}$, $Rh^{3+}$, $Pt^{3+}$, and $Pd^{2+}$.[28,30–32] In fact, recently we extended this approach to Am(vi) to study the nature of the first EXAFS measurement of an Am(vi)/Am(iii) mixture solution.[33] We were able to simulate independently EXAFS spectra of both the americyl cation and the Am(iii) aqua ion and combine them to simulate the theoretical EXAFS spectrum of an ion mixture in solution.

We present in this work a set of new *ab initio* interaction potentials for $[AnO_2 \cdot (H_2O)_5]^{2+/+}$ based on the HI model to provide a global picture of the influence that the oxidation state and element nature have on their aqua ion properties.

## II. METHODS

### A. Hydrated ion model potential for actinyls

The set of *ab initio* interaction potentials developed is based on the $[AnO_2 \cdot (H_2O)_5]^{2+/+}$ model for An = Np(v,vi), Pu(vi), Am(vi). We follow the methodology that has already been successful in our $[UO_2 \cdot (H_2O)_5]^{2+}$ study. Each actinyl potential has been developed as a particular case of the general method established for the uranyl case.[21]

The main feature of the HI model force fields is to consider two different types of water molecules: first-shell and bulk.[25,26] The first one bears strong polarization effects and partial charge transfer due to the direct interaction with the cation. The latter water molecules are bulk molecules, in this case modeled by the TIP4P potential.[34] First-shell water molecules will have different atom

types, partial charges, geometries, and non-electrostatic interactions than bulk water molecules. The main limitation in this model is that the release of a water molecule from the first shell renders the simulation system unphysical. Because, the actinyls studied have first-shell mean residence times (MRTs) much longer than the simulation time,[29,35,36] the HI model is very appropriate for these systems. All MD simulations carried out in this work have been monitored to check that the first-shell water molecules stay in their shell along the whole simulation. This monitorization is a requirement to guarantee the correct behavior of the potential when the model is employed.

All $H_2O$ molecules are treated as rigid bodies. Nevertheless, the hydrated ion is flexible in its first shell and also within the $[AnO_2]^{2+/+}$ unit. The potential energy of the whole simulation system is partitioned as follows:

$$E = E_{IMC} + E_{IW1} + E_{W_I-W_I} + E_{HIW} + E_{TIP4P}. \quad (1)$$

The terms that are fitted to the quantum mechanical (QM) information are $E_{IMC}$ (Intra-Molecular Cation) which accounts for the interactions within the $[AnO_2]^{2+/+}$ unit, $E_{IW1}$ (Ion-Water of the 1st shell) that provides the interaction of the molecular cation with its first shell, and $E_{HIW}$ (Hydrated Ion Water) which describes the interaction energy of bulk water molecules and $[AnO_2 \cdot (H_2O)_5]^{2+/+}$. The remaining terms are the Lennard-Jones plus the electrostatic interactions among bulk water molecules ($E_{TIP4P}$) and first-shell solvent molecules ($E_{W_I-W_I}$). The fitted terms have an electrostatic contribution in addition to a non-electrostatic component defined by a $\frac{C_{ij}}{r^n}$ polynomial functional form where $n = 4, 6, 8, 12$. The expressions for the potential terms are

$$E_{IMC} = \sum_i^{\substack{O_{yl} \\ sites}} \left( \frac{C_4^{AnO_{yl}}}{r_{AnO_{yl}}^4} + \frac{C_6^{AnO_{yl}}}{r_{AnO_{yl}}^6} + \frac{C_8^{AnO_{yl}}}{r_{AnO_{yl}}^8} + \frac{C_{12}^{AnO_{yl}}}{r_{AnO_{yl}}^{12}} \right) + \sum_i^{O_{yl}} \frac{q_{An} q_{O_{yl,i}}}{r_{AnO_{yl,i}}},$$

$$(2)$$

$$E_{IW1} = \sum_i^{\substack{AnO_2 \\ sites}} \frac{C_4^{iO_I}}{r_{iO_I}^4} + \frac{C_6^{iO_I}}{r_{iO_I}^6} + \frac{C_8^{iO_I}}{r_{iO_I}^8} + \frac{C_{12}^{iO_I}}{r_{iO_I}^{12}} + \sum_i^{AnO_2} \sum_j^{\substack{1^{st} \text{ shell Water} \\ sites}} \frac{q_i q_j}{r_{ij}}, \quad (3)$$

$$E_{HIW} = \sum_i^{\substack{HI \\ sites}} \sum_j^{Watersites} \left( \frac{C_4^{ij}}{r_{ij}^4} + \frac{C_6^{ij}}{r_{ij}^6} + \frac{C_8^{ij}}{r_{ij}^8} + \frac{C_{12}^{ij}}{r_{ij}^{12}} + \frac{q_i q_j}{r_{ij}} \right). \quad (4)$$

The structures used to parameterize the IMC and IW1 potentials always contain the pentahydrate in the gas phase and are deformations following the normal modes of bending and symmetric or antisymmetric stretching. The fact of including first-shell water molecules in the QM calculations guarantees the polarization of the actinyl and the first-shell water molecules of the hydrated ion entity as present in solution. In the case of the HIW potential, the structures to parameterize the potential consist of the pentahydrate and a single bulk water molecule. The additional polarization of the rest of the solution will be provided in the simulation by the HIW term. Details of the procedure can be found elsewhere.[21]

Due to the low degree of polarization and charge transfer in the case of $[NpO_2 \cdot (H_2O)_5]^+$, the first-shell water molecules bear

the same charges and geometry as the TIP4P water model (including the massless point charge). Nevertheless, they are still different from bulk water molecules due to the non-electrostatic part of the IW1 and HIW interaction potentials. The IW1 and IMC interaction potentials were fitted specifically for each of the actinyl species, whereas the non-electrostatic part of the HIW potential developed for $[UO_2 \cdot (H_2O)_5]^{2+}$ was transferred for all actinyls. This assumption was based on the previous experience of the group with other cations[28,30–33] and the fact that actinyls have a similar coordination chemistry. To test this, in Fig. 1, we present scans of the interaction energy of a second-shell water molecule with the HI obtained from QM calculations and the HIW potential. The ions $[NpO_2 \cdot (H_2O)_5]^{2+}$ and $[NpO_2 \cdot (H_2O)_5]^{+}$ were chosen as representatives of the set, but analogous results were obtained for the other actinyls. The approximation is reasonable since the difference between the curves has the same magnitude as the typical uncertainty associated with the fitting of the *ab initio* interaction potentials. Furthermore, the error of the pentavalent case is nearly constant, as a consequence the equations of motion are not altered given that these equations are propagated using the gradient of the potential.

All the parameters of the interaction potentials can be found in Tables S1-S5 of the supplementary material.

The level of theory of the PES used to fit the interaction potentials is the same as in our previous work: B3LYP[37,38]/aug-cc-PVDZ[39] with Stuttgard relativistic effective core pseudopotentials[40] using Gaussian09.[41] Partial charges were calculated using the Merz-Kollman[42,43] method polarizing previously the electronic density with the Polarizable Continuum Model (PCM) of solvation.[44] The B3LYP functional has given reliable interaction energies and molecular geometries for actinyls[45–47] even if they have an open-shell nature.[48,49] Some NEVPT2[50–52] geometrical scans were carried out using the ORCA package[53] in order to test this issue. The ground state multiplicities of the aqua ions are a doublet for
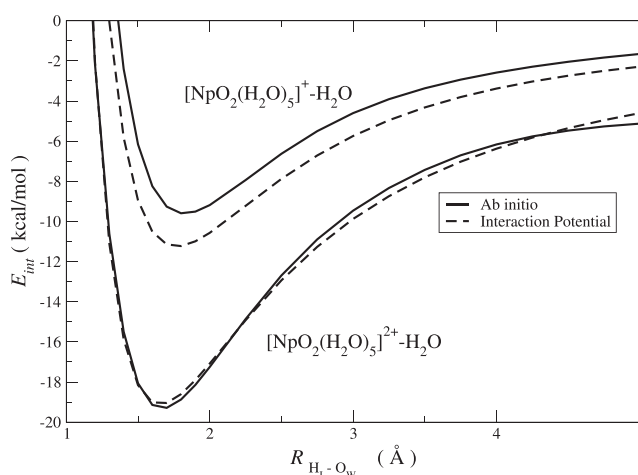
$NpO_2^{2+}$, a triplet for $NpO_2^{+}$ and $PuO_2^{2+}$, and a quartet for $AmO_2^{2+}$. The active space chosen was four $\pi/\pi^*$ and two $\sigma/\sigma^*$ molecular orbitals formed by actinoid f-orbitals and p-orbitals of the $O_{yl}$ atoms and 4 atomic-like non-bonding f-orbitals of the actinoid. This led to CASSCF(n,10) configurations where n is 6 plus the number of actinoid unpaired electrons. The addition of bonding and antibonding molecular orbitals is motivated by the fact that f-orbitals participate in the formation of the oxo-bond. These orbitals were obtained from small-basis set unrestricted Density Functional Theory (DFT) calculation using the Becke-Perdew (BP) functional and using the "stable" keyword as recommended in the ORCA CASSCF tutorial (http://www.molphys.org/orca_tutorial/orca_hands_on.html). Since the ground states are degenerate, the calculations were run using a state average over the degenerate states excluding excited states. The perturbational step of the calculation was done using quasi-degenerate perturbation theory. The basis sets used were ma-def2-TZVP for O, def2-SVP for H, and SD(60,MWB)//DEF-TZVP for actinides.[40,54] The calculations were accelerated using the RI and RIJK pseudospectral methods with "autoaux" auxiliary basis sets. Figure S1 of the supplementary material shows four geometry scans at both levels of theory. In all cases, the differences using B3LYP or NEVPT2 level of calculation were in the range of the typical fit root mean square error of our *ab initio* force fields. Furthermore, the optimized geometry bond lengths at the NEVPT2 level differ less than 3% which is irrelevant for most solution properties. These small differences are in part due to the fact that unrestricted DFT computations include static electron correlation using a mean field approach which seems sufficient for our purposes.

## B. Molecular dynamics simulations

For each of the actinyl species, the simulated system consisted of a hydrated ion, $[AnO_2 \cdot (H_2O)_5]^{2+/+}$, and 1495 TIP4P water molecules initially at pure water density and an approximate ion concentration of ~0.04 mol kg$^{-1}$. A 5 ns NPT trajectory was integrated using the velocity Verlet and the NOSQUISH[55] quaternion algorithms with a 1 fs time step. 0.5 ns of equilibration was performed. The average temperature and pressure were kept constant at 300 K and 1 atm using the Nosè Hoover barostat and thermostat with characteristic times of 0.5 ps. Short range interactions were truncated at 14 Å, and electrostatic interactions were calculated using the Ewald sum. The simulations were performed using a modified version of DL_POLY Classic[56] which includes the functional forms of the new potential developed.

## III. RESULTS AND DISCUSSION

### A. Hydration enthalpies

The hydration enthalpies, $\Delta H_{hyd}$, of $[AnO_2]^{2+/+}$ were obtained by the following expression:

$$\Delta H_{hyd} = H_{[AnO_2]^{2+/+}(aq)} - H_{H_2O(aq)} - H_{[AnO_2]^{2+/+}(g)}, \quad (5)$$

where $H_{[AnO_2]^{2+/+}(aq)}$, $H_{H_2O(aq)}$, and $H_{[AnO_2]^{2+/+}(g)}$ are the MD simulation enthalpies of the aqua ion solution (one ion and 1500 solvent molecules), a 1500 $H_2O$ box, and $[AnO_2]^{2+/+}(g)$. Table I contains the results.



**FIG. 1**. Interaction energy scans of a bulk water molecule with $[NpO_2 \cdot (H_2O)_5]^{+}$ (top) and $[NpO_2 \cdot (H_2O)_5]^{2+}$ (bottom) obtained with B3LYP calculations (solid lines) or the HIW potential (dashed lines). The HIW potential was parameterized for $[UO_2 \cdot (H_2O)_5]^{2+}$ in our previous work[21] and was extrapolated to other hexavalent and pentavalent actinyls.

**TABLE I**. Energetic, structural, and dynamical properties calculated from the molecular dynamics simulations. Uncertainties are standard errors.

| Property | U(VI) | Np(VI) | Np(V) | Pu(VI) | Am(VI) |
|---|---|---|---|---|---|
| $\Delta H_{hyd}$ (kcal mol$^{-1}$) | $-333 \pm 14$ | $-337 \pm 14$ | $-190 \pm 16$ | $-350 \pm 16$ | $-342 \pm 16$ |
| $D_{An}(10^{-5})$ cm$^2$ s$^{-1}$ | $1.2 \pm 0.2$ | $1.2 \pm 0.2$ | $1.2 \pm 0.1$ | $1.2 \pm 0.1$ | $1.3 \pm 0.1$ |
| $D_{An}/D_W$ | $0.37 \pm 0.04$ | $0.38 \pm 0.03$ | $0.36 \pm 0.06$ | $0.38 \pm 0.03$ | $0.39 \pm 0.03$ |
| $r_{An-O_{yl}}$ (Å) | 1.77 | 1.73 | 1.79 | 1.72 | 1.72 |
| $r_{An-O_{I}}$ (Å) | 2.46 | 2.43 | 2.58 | 2.43 | 2.44 |
| $r_{An-O_{II}}$ (Å) | 4.61 | 4.63 | 4.74 | 4.60 | 4.64 |
| $CN_{An-O_{II}}$ | 22 | 25 | 22 | 22 | 22 |
| MRT$_W$ (ps), $t^* = 0$ ps | $8 \pm 1$ | $6.9 \pm 0.2$ | $5.1 \pm 0.3$ | $8 \pm 1$ | $8 \pm 1$ |
| MRT$_W$ (ps), $t^* = 2$ ps | $17 \pm 1$ | $15.9 \pm 0.5$ | $13.4 \pm 0.5$ | $16 \pm 1$ | $16 \pm 1$ |

All the hexavalent enthalpies are statistically identical and vary around −340 kcal/mol. In the case of [NpO$_2$]$^+$, $\Delta H_{hyd}$ is −190 kcal/mol, about 40% less than the corresponding [NpO$_2$]$^{2+}$ value.

Gibson et al.[57] measured the hydration enthalpies of all the hexavalent actinyls studied, obtaining values around −400 kcal mol. Marcus[58] obtained a value of −325 ± 5 kcal mol$^{-1}$ for [UO$_2$]$^{2+}$, 75 kcal mol$^{-1}$ smaller than Gibson's value. The difficulty of measuring the formation enthalpy of gas phase actinyl ions might be, in part, the cause of this discrepancy.[59] This difficulty is even stronger in the case of the dication since it involves measuring the second ionization energy of the gas phase actinyl. Our value for the hexavalent actinyls approaches the value of Marcus especially since our $H_{[AnO_2]^{2+/+}}$ could be missing a small many-body contribution in the first-second shell interaction.[26] The [NpO$_2$]$^+$ hydration enthalpy from MD matches Gibson's value experimental value of −180 ± 20 kcal mol$^{-1}$. Rai et al.[17] have computed $\Delta G_{hydr}$ for the uranyl based on an integration path split into two steps, growth and charging of the actinyl cation in water. Their $\Delta G_{hydr}$ values obtained for different water models are in between the reported experimental data.[57,58]

### B. Self-diffusion coefficient

The translational self-diffusion coefficients, $D_0$, of the actinyls were calculated using the Einstein equation and correcting for finite box-size effects with the formula of Yeh and Hummer,[60]

$$D_{An}^{corr} = D_{An}^0 + \frac{k_B T \xi}{6\pi\eta L}, \qquad (6)$$

where $\eta$ is the TIP4P water viscosity, $L$ is the box length, and $\xi$ is the self-term for a cubic box (2.8373 at room temperature). This correction is significant in the absolute value, and thus uncorrected $D_{An}^0$ values are in the range 0.8-0.9 × 10$^{-5}$ cm$^2$ s$^{-1}$, whereas size-corrected diffusion data are in the range 1.2-1.3 × 10$^{-5}$ cm$^2$ s$^{-1}$ (Table I). Uncorrected $D_{An}^0$ values obtained by Tiwari et al.[61] are in the range 0.6-0.7 × 10$^{-5}$ cm$^2$ s$^{-1}$ using SPC/E for the water model. The diffusion coefficient of a solute correlates strongly with the solvent diffusion. Bearing in mind that the TIP4P water model overestimates the water mobility, the comparison between ion mobilities derived from this work and that of Tiwari et al.[61] is satisfactory. For the particular case of uranyl, Kerisit and Liu[62]

using three different potentials and the SPC/E model for water give uncorrected $D_{An}^0$ values in the range 0.85-0.94 × 10$^{-5}$ cm$^2$ s$^{-1}$. To supply a less dependent $D_{An}$ on the water mobility, it is common practice in the literature[61–63] that the solute diffusion coefficients are normalized by the water self-diffusion coefficient.

The experimental self diffusion coefficients of the different actinyls range from 0.55 × 10$^{-5}$ cm$^2$ s$^{-1}$ to 0.8 × 10$^{-5}$ cm$^2$ s$^{-1}$.[64–66] Considering TIP4P water mobility is too high, the aqua ion translates more freely than it should as well. The normalization corrects this effect, and then the data agree within the error with the experimental normalized range, 0.24-0.35,[64,65] using 2.3 × 10$^{-5}$ cm$^2$ s$^{-1}$ for water.[67]

We observe once again how our MD results reflect the physicochemical similarity among the different actinyls. Surprisingly, the difference in $D^0$ for the Np(VI)/Np(V) pair is small experimentally[64] (~0.8 and ~0.7 × 10$^{-5}$ cm$^2$ s$^{-1}$) and in our model, a common value (~1.2 × 10$^{-5}$ cm$^2$ s$^{-1}$), despite the difference in the solute-solvent interaction strength manifested by the $\Delta H_{hyd}$ values. Thus, the hydrodynamic radius dominates actinyl diffusion, which is very similar for both mono- and di-valent cations, in fact the minimum for the Np–O radial distribution functions (RDFs) enclosing the first hydration shell are 6.3 and 6.0 Å for Np(V) and Np(VI), respectively.

### C. Normal mode frequencies

The MD and experimental normal mode frequencies of the aqua ions in solution are presented in Table II. The selected normal modes are the symmetric and antisymmetric An–O$_{yl}$ stretching of the irreducible representation $1A_1$ and $A_2$, respectively; the actinyl bending, $E_1$, and the water breathing stretching $2A_1$. The frequencies were calculated from the Fourier transforms of the velocity autocorrelation functions of generalized coordinates associated with these motions. Details of the procedure can be found elsewhere.[21] Unlike most force fields, our normal mode frequencies incorporate all the anharmonicities of the ab initio potential energy surface.

Our frequencies agree reasonably with the experiment having a maximum relative error of 15%. All the frequencies overestimate the infrared and Raman spectroscopy data. A bias of the B3LYP potential energy surface could cause this. The hydrated uranyl ion

**TABLE II**. Experimental and MD normal mode frequencies in $cm^{-1}$. The uncertainty of the results is $\pm 5$ $cm^{-1}$. All experimental symmetric and antisymmetric values are from Refs. 68 and 69, respectively.

| System | Method | $E_1$ | $2A_1$ | $1A_1$ | $A_2$ |
|---|---|---|---|---|---|
| $[UO_2 \cdot (H_2O)_5]^{2+}$(aq) | MD | 252 | 338 | 1004 | 1101 |
| | Expt. | $253 \pm 10$ | | $870 \pm 10$ | $965 \pm 1$ |
| $[NpO_2 \cdot (H_2O)_5]^{2+}$(aq) | MD | 265 | 374 | 976 | 1073 |
| | Expt. | | | $863 \pm 5$ | $969 \pm 1$ |
| $[NpO_2 \cdot (H_2O)_5]^{+}$(aq) | MD | 295 | 270 | 839 | 875 |
| | Expt. | | | $824 \pm 4$ | $863 \pm 5$ |
| $[PuO_2 \cdot (H_2O)_5]^{2+}$(aq) | MD | 297 | 361 | 890 | 1048 |
| | Expt. | | | $835 \pm 5$ | $962 \pm 1$ |
| $[AmO_2 \cdot (H_2O)_5]^{2+}$(aq) | MD | 309 | 353 | 882 | 957 |
| | Expt. | | | | $939 \pm 1$ |

gas phase QM frequencies (within the harmonic approximation) are 224 $cm^{-1}$, 314 $cm^{-1}$, 945 $cm^{-1}$, and 1028 $cm^{-1}$ for $E_1$, $2A_1$, $1A_1$, and $A_2$, respectively. If the frequencies are calculated from a gas phase simulation of hydrated uranyl using the classical force field at 300 K, the values obtained are 256 $cm^{-1}$, 286 $cm^{-1}$, 977 $cm^{-1}$, and 1027 $cm^{-1}$ for $E_1$, $2A_1$, $1A_1$, and $A_2$, respectively. The comparison between these two sets of frequencies proves that the bias in the frequencies is due to the level of theory and not to the ability of the potential to reproduce the PES. The frequencies of the interaction potential even in a perfect fit situation are always going biased by the quantum-mechanical level used to calculate the PES. This means, if it was necessary to improve normal mode frequencies prediction, our force field development procedure could be used with a higher level of theory.

### D. Hydration structure of actinyls in aqueous solution

The properties involving the second hydration shell of the hexavalent actinyls are statistically equivalent since all An(VI) present similar An–O distances (Table I) and their radial distribution functions nearly overlap (see Fig. S2 in the supplementary material). Our An–O distances agree with those obtained by Maginn and col.[24] from molecular dynamic simulations using their model force field within the hundredth of an angstrom. Due to this strong analogy of the hexavalent aqua ions, the conclusions of our previous work on uranyl[21] generalize to all actinyl dications as we have found for diffusion and hydration enthalpies. Our model describes the hydration of hexavalent actinyls as cations which equatorially have conventional monoatomic cation solvation and axially hydrophobic caps around the $O_{yl}$ oxygens. Figure 2 depicts this behavior where two simulation snapshots of U(VI) with second-shell equatorial water molecules colored in blue [Fig. 2(a)] and axial water molecules in orange [Fig. 2(b)] are shown. Equatorial water molecules form typical hydrogen bonds (HBs) with first-shell water molecules as present in most metal cations. By contrast, axial solvent molecules form HB with other solvent molecules around the $O_{yl}$ atoms but without directly interacting with it. This last type of solvation is analogous to that of *hydrophobic* solutes like methane.[70] Figure 3 shows the Spatial Distribution Function (SDF) of bulk water oxygen atoms around

the hydrated ion, and the presence of different solvation zones is clear.

We will now compare the hydration structure of the Np(VI)/Np(V) revealing the effect of the charge. Figure 4 shows the Np–O and Np–H radial distribution functions (RDFs) of the neptunyl aqua ion in both oxidation states. Np–O RDFs [Fig. 4(a)] show the intense peaks corresponding to first-shell atom types: $O_{yl}$, $O_I$. Both radial distributions have very similar shapes except for a slightly lower intensity and a shift toward longer distances in Np(V). The Np–O distances are longer for Np(V) than for Np(VI) as a consequence of the smaller charge. This effect is more pronounced for the first and second hydration shells which lengthen their Np–O distances 0.15 Å and 0.11 Å, when going from $NpO_2^{2+}$ to $NpO_2^+$, than for the Np–$O_{yl}$ distance that only increases 0.06 Å. This may be understood on the basis that the Np–O interactions are mostly electrostatic, whereas the Np–$O_{yl}$ oxo bonds are mostly covalent.

The integration of the Np–$O_W$ RDFs up to their second shell minima (6.0 Å for $NpO_2^{2+}$ and 6.3 Å $NpO_2^+$) gives running integration numbers of 29 for Np(VI) and 32 for Np(V). As happened in $[UO_2]^{2+}$,[21] the Np(VI) value is higher than for the rest of
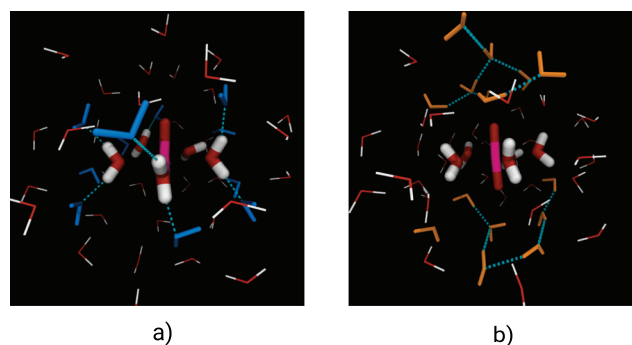


FIG. 2. Images (a) and (b) are snapshots of the MD trajectory highlighting equatorial (blue) and axial (orange) second-shell water molecules of the actinyl hexavalent aquaion.
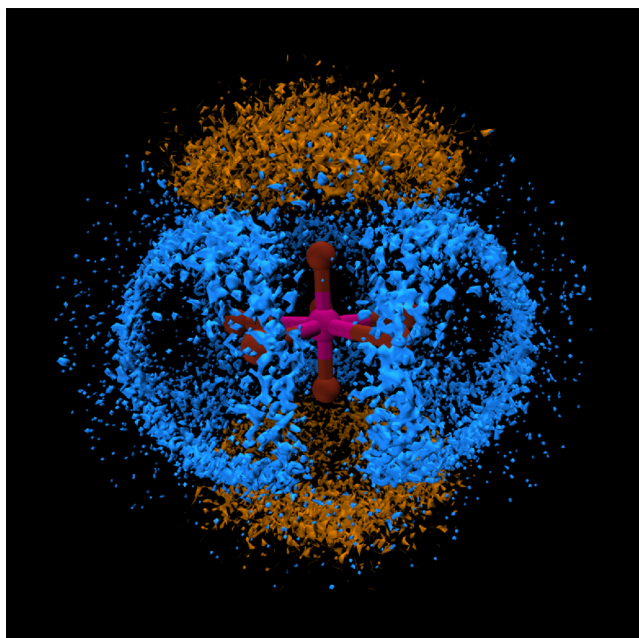
**FIG. 3**. Spatial distribution function (SDF) of solvent molecules around the actinyl hexavalent aquaion. The axial solvation shell is colored in orange and the equatorial solvation shell in blue.

charged monoatomic cations are expected on average to form two HBs with the second shell therefore having in the second shell about twice the number of first-shell water molecules.[71,72] Our values are about three times the first-shell coordination number.

Actinyls have a non-spherically symmetric complex hydration structure. The use of a spherically averaged function like the total RDF may lead to a misinterpretation, in the present case overestimating the CN. If the total An–O RDF is integrated up to ~6.3 Å [see Fig. 4(a)], it will include the true first shell of water molecules (axial and equatorial) but also the intermediate ones which may be assigned to either. A proper CN can be computed avoiding this artifact by using the multisite cavity CN definition which is adequate for non-spherical solvation environments.[73] The multisite cavity CN is defined as the average number of water molecules within overlapping spheres centered on solvent-exposed atoms ($O_{yl}$ and $O_I$). The radii of these spheres correspond to the minima above the first peak of angle-solved X–$O_W$ RDFs. This multisite cavity contains the molecules that must be considered primarily to be solvating the $[AnO_2 \cdot (H_2O)_5]^{2+/+}$ cation. With this definition, the second shell CN for Np(VI)/Np(V) is, respectively, 22 and 25. We attribute the difference in CN to the uncertainty in the definition of the cavity radii. These values are close to the values of the literature obtained by integrating the total RDF and are consistent with our analysis of the angle-solved RDFs. Our actinyl models have more anisotropic hydration than those of the literature which creates a larger discrepancy between RDF-CN and multisite cavity CN. The cause for this is the specific charge transfer and polarization suffered by the first-shell water molecules which unlike other classical potentials are different from bulk water molecules. The other possible way to explicitly include this charge transfer in simulation would be to use *ab initio* MD simulations, but its computational cost is too high to study systems big enough to accommodate a well defined second

literature values, both theoretical[13–15,18–20,24] and experimental[3,16] which oscillate between 14 and 19. No experimental values are available for Np(V), the CPMD simulation of Odoh *et al.*[22] on $[PuO_2]^+$ gives a value of ~22. First-shell water molecules of typical highly



a)



b)
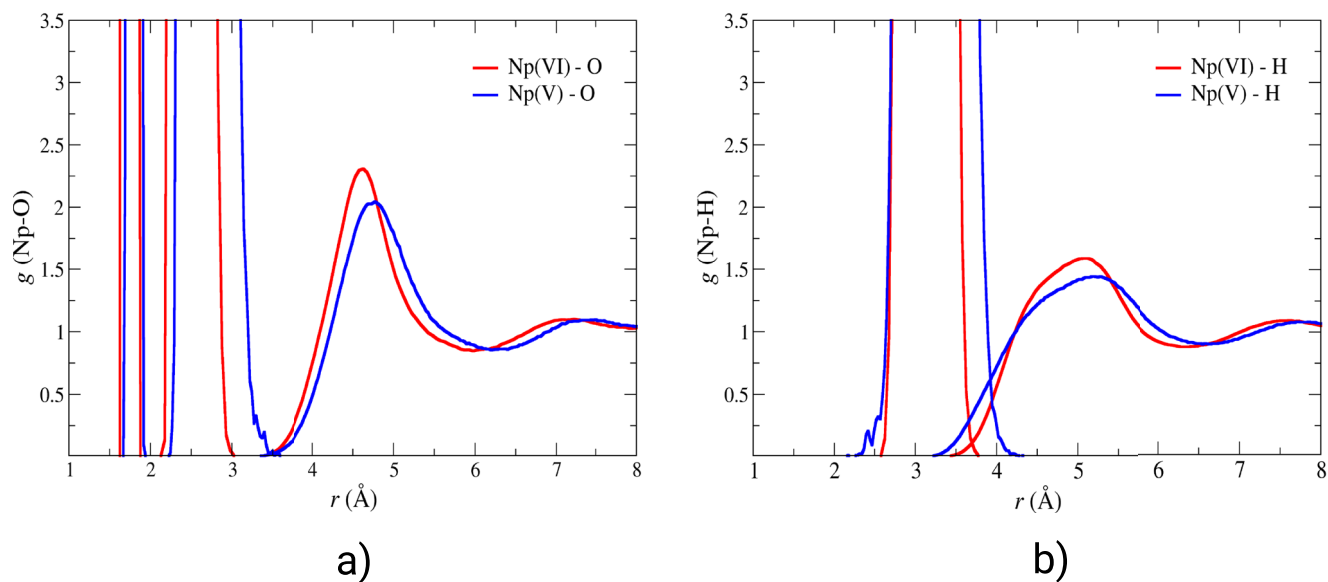
**FIG. 4**. An–O (a) and An–H (b) RDFs for $[NpO_2 \cdot (H_2O)_5]^{2+}$ (red) and $[NpO_2 \cdot (H_2O)_5]^+$ (blue).

shell. This issue has been examined in greater detail in our previous studies.[21,73]

As previously discussed, portraying actinyls with total RDFs can lead to artifacts in the analysis. Therefore, three hydration regions are defined using the molecular axis of the actinyl as reference. The axial region is defined by azimuthal angles from $0°$ to $30°$ with respect to both $Np–O_{yl}$ [Fig. 5(c)]. Likewise, the intermediate and equatorial regions scan the angular ranges of $30°$-$60°$ and $60°$-$90°$, respectively. The $Np–X$ angle-solved RDFs and the region definitions are given in Fig. 5.

The equatorial $Np–O_W$ RDFs have maxima at 4.62 Å for $Np(VI)$ and 4.74 Å for $Np(V)$ both integrating to 10 water molecules. The relative position of the equatorial $Np–H_W$ RDFs with respect to $O_W$ shows that equatorial second-shell water molecules form well defined HBs with the first hydration shell. Both these facts depict an equatorial solvation shell that follows the typical monoatomic cation structure. The main differences between the RDFs of $Np(VI)$ and $Np(V)$ is that the RDF of the pentavalent cation second-shell peaks 0.1 Å further away and that ends with an inflexion point at 5.5 Å, and not a minimum, lacking a third solvation shell [see bottom of Fig. 4(b)]. The inflection point evidences that the water structure becomes bulk-like immediately after the second-shell as is the case for other monovalent cations.[74,75] For $Np(VI)$, the structure-making effect of the cation is more long ranged and even a third solvation shell is weakly observed.

The axial and intermediate angle-solved RDFs are similar for both oxidation states (see top and center plots in Fig. 5). Their main difference is that the axial $Np(V)–H_W$ angle-solved RDF is broader and approaches more the central atom. The coordination numbers for the axial and intermediate regions are 4 and 12 regardless of the aqua ion charge. For both valencies, the equatorial second-shell ends at shorter distances than the total RDF. Thus the integration of the total RDF captures hydration not only from the equatorial region but also from the axial and intermediate shells whose RDFs finish more than 1 Å further away. The intermediate region plays the role of a bridge that smoothly transitions the solvent behavior from axial to equatorial.

The absence or presence of solvent HBs with the $O_{yl}$ atom is an ongoing debate in the literature[13–20,24] because it would define the $O_{yl}$ atom as *hydrophobic* or *hydrophillic*. In our $[UO_2 \cdot (H_2O)_5]^{2+}(aq)$ model,[21] there was no HB formation and clathrate-like structures were observed in the axial regions. In these structures, water molecules form HB among them rather than with the $O_{yl}$ atom [see Fig. 2(b)]. In Fig. 6, we present the angle-solved $O_{yl}–X$ RDFs for the $0°$-$90°$ region of $[NpO_2 \cdot (H_2O)_5]^{2+/+}(aq)$. For both oxidation states, the overall shapes are similar. The RDFs have features that led to the same conclusion: the water molecules are far away from the $O_{yl}$ atom ($\sim$3.5 Å) and the $O_{yl}–H_W$ and $O_{yl}–O_W$ overlap significantly, i.e., there is no preferential water orientation involving HBs with $O_{yl}$. In summary, across the series and for both oxidation states, the axial



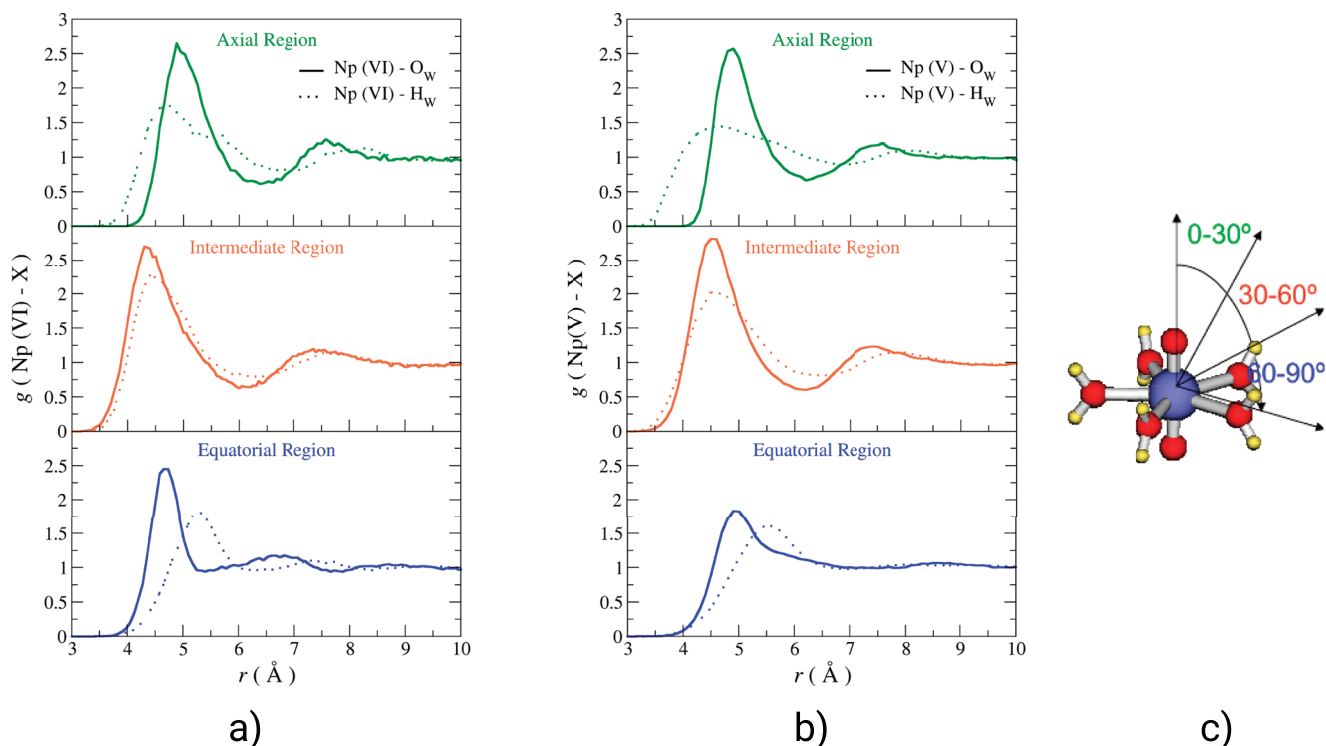**FIG. 5**. An–$O_W$ (solid lines) and An–$H_W$ (dotted lines) angle-solved ($0°$-$90°$) RDF for $[NpO_2 \cdot (H_2O)_5]^{2+}$ (a) and $[NpO_2 \cdot (H_2O)_5]^+$ (b) for their axial, intermediate, and equatorial regions. (c) defines the angular regions of $[AnO_2]^{2+/+}$.
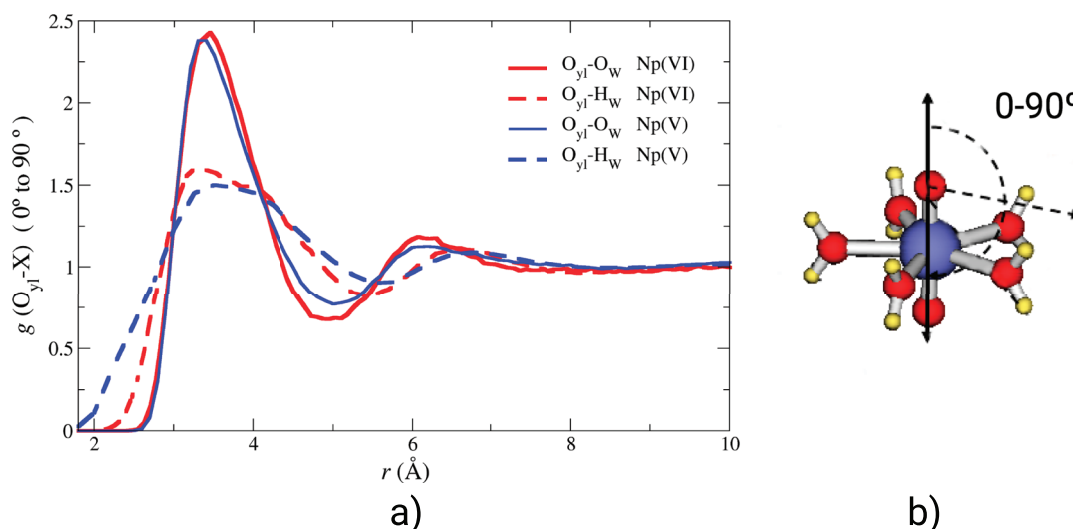
FIG. 6. (a) $O_{yl}$–$O_W$ (solid lines) and $O_{yl}$–$H_W$ (dotted lines) angle-solved RDFs (0-90) in $[NpO_2 \cdot (H_2O)_5]^{2+}$ (red) and $[NpO_2 \cdot (H_2O)_5]^{+}$ (blue). (b) defines the angular regions of the $O_{yl}$ atom.

region is *hydrophobic* and no HB formation with the $O_{yl}$ atom is observed.

The overall picture of the actinyls studied in this work is similar to $[UO_2 \cdot (H_2O)_5]^{2+}$. The aqua ion has the typical monoatomic cation second-shell hydration structure equatorially and is capped at the poles by clathrate-like regions.

### E. Second-shell water mean residence times

Mean residence times (MRTs) for the second-shell water molecules were calculated using the method of Impey et al.[76] With this method, the water molecules are allowed for leaving the shell and return for a time $t^*$ without loosing their assignment to the region. We use the values of $t^*_{2nd\,shell} = 0$ ps and 2 ps which are the most common values in the literature[76,77] and allow us to establish a reasonable range to estimate this property. The MRTs of the different hexavalent actinyls are statistically identical (see Table I). Therefore, as we have established

for most of the properties, the conclusions obtained previously for uranyl[21] apply to the other elements. We will now compare Np(VI) and Np(V) to discuss the charge effect on the MRT, and their values are collected in Table III.

The total MRT for second-shell water molecules of $[NpO_2 \cdot (H_2O)_5]^{2+}$ is higher than for other doubly charged atomic cations like $Mg^{2+}$ where typical values are 3 ps and 14 ps for $t^*_{2nd\,shell} = 0$ ps and 2 ps, respectively.[28] But it is surprising that despite its lower charge, $[NpO_2 \cdot (H_2O)_5]^{+}$ also has total MRTs higher than $Mg^{2+}$. This is mostly likely due to the large volume of the $[NpO_2]^{2+/+}$ second shell which is comparable for both oxidation states.

If we compare the angle-solved MRTs of the two oxidation states, we obtain the same ordering of the regions. For $t^*_{2nd\,shell} = 2$ ps, in particular, the region with the highest MRT is the equatorial region, followed by the intermediate region and the axial region, since the equatorial and bridge regions can form HBs with the first shell and the axial region is dominated by water-water interactions. The most remarkable feature of the MRTs is that in both cases for

TABLE III. Mean residence times (ps) of $H_2O$ in the second shell of $[NpO_2]^{2+/+]}$ obtained with the method of Impey et al.[76] and their decomposition in the angular regions of Fig. 5(c). MRTs of TIP4P water in the first shell of another water molecule in pure water are ~1.4 ps and ~4.2 ps for $t^* = 0$ ps and $t^* = 2$ ps, respectively. The uncertainties are standard errors.

| System | $[NpO_2 \cdot (H_2O)_5]^{2+}$ | | $[NpO_2 \cdot (H_2O)_5]^{+}$ | |
| --- | --- | --- | --- | --- |
| | $t^*_{2ndshell} = 0$ ps | $t^*_{2ndshell} = 2$ ps | $t^*_{2nd\,shell} = 0$ ps | $t^*_{2ndshell} = 2$ ps |
| Total | 6.9 ± 0.2 | 15.9 ± 0.5 | 5.1 ± 0.3 | 13.4 ± 0.5 |
| 0°-30° (axial) | 0.79 ± 0.04 | 4.8 ± 0.4 | 0.60 ± 0.02 | 4.6 ± 0.2 |
| 30°-60° (intermediate) | 0.60 ± 0.01 | 6.88 ± 0.07 | 0.47 ± 0.01 | 6.9 ± 0.6 |
| 60°-90° (equatorial) | 1.41 ± 0.04 | 8.6 ± 0.2 | 1.66 ± 0.06 | 9.9 ± 0.2 |

$t^{*}_{\text{2nd shell}}$ = 2 ps, the axial MRT is larger than the MRT of a TIP4P water molecule in the first-shell of another water molecule. Therefore, there is a local reinforcement of the water structure around the $O_{yl}$ atom without direct interaction with it. This is a dynamical property characteristic of clathrate-like hydration around a hydrophobic solute.[70,78]

## IV. CONCLUSIONS

We have successfully applied the hydrated ion methodology developed for U(VI)[21] to the actinyl series by changing both the charge and the actinide element. The IW1 and IMC interaction potentials in addition to a transferred HIW potential from $[UO_2]^{2+}$ correctly model the potential energy surface.

The simulation results agree satisfactorily with experimental evidence of multiple nature: structural, dynamical, and thermodynamical, validating therefore interaction potentials for further studies. Besides first-shell distances, the solvation properties of all hexavalent actinyls are indistinguishable, despite the specificity of the IW1 potential and partial charges. This suggests the possibility of using the uranyl cation as a reference for the study of systems where other actinyls are involved as long as the integrity of the aqua ion is preserved. Comparing Np(VI) and Np(V), we found that their structure and dynamics are rather similar apart from the logical small lengthening of An–$O_{yl}$ and An–$O_W$ distances and a small shortening in second shell MRTs due to the decrease in the total charge.

The hydration picture of a general An(V,VI) is remarkably similar to that of U(VI). Actinyls are anisotropic amphiphilic solutes which display a conventional metal ion equatorial solvation shell capped at the poles by clathrate-like solvent structures, mediated by bridge water molecules in the intermediate regions.

## SUPPLEMENTARY MATERIAL

See supplementary material for all the actinyl hydrated ion force field parameters, additional RDFs, and interaction energy scans.

## ACKNOWLEDGMENTS

## REFERENCES

[1] S. Cotton, *Lanthanide and Actinide Chemistry* (Wiley, London, 2006).

[2] C. M. N. Bardin and P. Rubini, Radiochim. Acta **83**, 189 (1998) and references therein.

[3] M. Aaberg, D. Ferri, J. Glaser, and I. Grenthe, Inorg. Chem. **22**, 3986 (1983).

[4] P. G. Allen, J. J. Bucher, D. K. Shuh, N. M. Edelstein, and T. Reich, Inorg. Chem. **36**, 4676 (1997).

[5] S. D. Conradson, Appl. Spectrosc. **52**, 252A (1998).

[6] U. Wahlgren, H. Moll, I. Grenthe, B. Schimmelpfennig, L. Maron, V. Vallet, and O. Gropen, J. Phys. Chem. A **103**, 8257 (1999).

[7] J. Neuefeind, L. Soderholm, and S. Skanthakumar, J. Phys. Chem. A **108**, 2733 (2004).

[8] L. Soderholm, S. Skanthakumar, and J. Neuefeind, Anal. Bioanal. Chem. **383**, 48 (2005).

[9] J. M. McKibben, Radiochim. Acta **36**, 3 (1984).

[10] M. Altmaier, X. Gaona, and T. Fanghänel, Chem. Rev. **113**, 901 (2013).

[11] C. Riddle, K. Czerwinski, E. Kim, P. Paviet, P. Weck, F. Poineau, and S. Conradson, J. Radioanal. Nucl. Chem. **309**, 1087 (2016).

[12] K. Maher, J. R. Bargar, and G. E. Brown, Inorg. Chem. **52**, 3510 (2013).

[13] P. Guilbaud and G. Wipff, J. Phys. Chem. **97**, 5685 (1993).

[14] P. Guilbaud and G. Wipff, J. Mol. Struct.: THEOCHEM **366**, 55 (1996).

[15] S. Kerisit and C. Liu, Geochim. Cosmochim. Acta **74**, 4937 (2010).

[16] D. Hagberg, G. Karlström, B. O. Roos, and L. Gagliardi, J. Am. Chem. Soc. **127**, 14250 (2005).

[17] N. Rai, S. P. Tiwari, and E. J. Maginn, J. Phys. Chem. B **116**, 10885 (2012).

[18] P. Nichols, E. J. Bylaska, G. K. Schenter, and W. de Jong, J. Chem. Phys. **128**, 124507 (2008).

[19] R. J. Frick, T. S. Hofer, A. B. Pribil, B. R. Randolf, and B. M. Rode, J. Phys. Chem. A **113**, 12496 (2009).

[20] M. Bühl, H. Kabrede, R. Diss, and G. Wipff, J. Am. Chem. Soc. **128**, 6357 (2006).

[21] S. Pérez-Conesa, F. Torrico, J. M. Martínez, R. R. Pappalardo, and E. Sánchez Marcos, J. Chem. Phys. **145**, 224502 (2016).

[22] S. O. Odoh, E. J. Bylaska, and W. A. De Jong, J. Phys. Chem. A **117**, 12256 (2013).

[23] R. Car and M. Parrinello, Phys. Rev. Lett. **55**, 2471 (1985).

[24] V. Pomogaev, S. P. Tiwari, N. Rai, G. S. Goff, W. Runde, W. F. Schneider, and E. J. Maginn, Phys. Chem. Chem. Phys. **15**, 15954 (2013).

[25] R. R. Pappalardo and E. Sánchez Marcos, J. Phys. Chem. **97**, 4500 (1993).

[26] R. R. Pappalardo, J. M. Martínez, and E. Sánchez Marcos, J. Phys. Chem. **100**, 11748 (1996).

[27] J. M. Martínez, R. R. Pappalardo, and E. Sánchez Marcos, J. Chem. Phys. **109**, 1445 (1998).

[28] J. M. Martínez, R. R. Pappalardo, and E. Sánchez Marcos, J. Am. Chem. Soc. **121**, 3175 (1999).

[29] D. T. Richens, *The Chemistry of Aqua Ions* (J. Wiley, West Sussex, England, 1997).

[30] J. M. Martínez, F. Torrico, R. R. Pappalardo, and E. Sánchez Marcos, J. Phys. Chem. B **108**, 15851 (2004).

[31] F. Torrico, R. R. Pappalardo, E. S. Marcos, and J. M. Martínez, Theor. Chem. Acc. **115**, 196 (2006).

[32] F. Carrera, F. Torrico, D. T. Richens, A. Muñoz-Páez, J. M. Martínez, R. R. Pappalardo, and E. Sánchez Marcos, J. Phys. Chem. B **111**, 8223 (2007).

[33] S. Pérez-Conesa, J. M. Martínez, R. R. Pappalardo, and E. Sánchez Marcos, Inorg. Chem. **57**, 8089 (2018).

[34] W. L. Jorgensen, J. Chandrasekhar, J. D. Madura, R. W. Impey, and M. L. Klein, J. Chem. Phys. **79**, 926 (1983).

[35] L. Helm and A. E. Merbach, Chem. Rev. **105**, 1923 (2005).

[36] A. F. Panasci, "Ligand exchange kinetics of environmentally relevant metals," Ph.D. thesis, University of California, Davis, 2014.

[37] A. D. Becke, J. Chem. Phys. **98**, 5648 (1993).

[38] P. J. Stephens, F. J. Devlin, C. F. Chabalowski, and M. J. Frisch, J. Phys. Chem. **98**, 11623 (1994).

[39] D. E. Woon and T. H. Dunning, Jr., J. Chem. Phys. **98**, 1358 (1993).

[40] W. Küchle, M. Dolg, H. Stoll, and J. Preuss, J. Chem. Phys. **100**, 7535 (1994).

[41] M. J. Frisch, G. W. Trucks, H. B. Schlegel, G. E. Scuseria, M. A. Robb, J. R. Cheeseman, G. Scalmani, V. Barone, B. Mennucci, G. A. Petersson, H. Nakatsuji, M. Caricato, X. Li, H. P. Hratchian, A. F. Izmaylov, J. Bloino, G. Zheng, J. L. Sonnenberg, M. Hada, M. Ehara, K. Toyota, R. Fukuda, J. Hasegawa, M. Ishida, T. Nakajima, Y. Honda, O. Kitao, H. Nakai, T. Vreven, J. A. Montgomery, Jr., J. E. Peralta, F. Ogliaro, M. Bearpark, J. J. Heyd, E. Brothers, K. N. Kudin, V. N. Staroverov, R. Kobayashi, J. Normand, K. Raghavachari, A. Rendell, J. C. Burant, S. S. Iyengar, J. Tomasi, M. Cossi, N. Rega, J. M. Millam, M. Klene, J. E. Knox, J. B. Cross, V. Bakken, C. Adamo, J. Jaramillo, R. Gomperts, R. E. Stratmann, O. Yazyev, A. J. Austin, R. Cammi, C. Pomelli, J. W. Ochterski, R. L. Martin, K. Morokuma, V. G. Zakrzewski, G. A. Voth, P. Salvador, J. J. Dannenberg, S. Dapprich, A. D. Daniels, Ö. Farkas, J. B. Foresman, J. V. Ortiz, J. Cioslowski, and D. J. Fox, GAUSSIAN09 Revision D.01, 2009.

[42] U. C. Singh and P. A. Kollman, J. Comput. Chem. **5**, 129 (1984).

[43] B. H. Besler, K. M. Merz, and P. A. Kollman, J. Comput. Chem. **11**, 431 (1990).

[44] J. Tomasi, B. Mennucci, and R. Cammi, Chem. Rev. **105**, 2999 (2005).

[45] B. Siboulet, C. J. Marsden, and P. Vitorge, Chem. Phys. **326**, 289 (2006).

[46] V. Vallet, P. Macak, U. Wahlgren, and I. Grenthe, Theor. Chem. Acc. **115**, 145 (2006).

[47] K. Balasubramanian and Z. Cao, Inorg. Chem. **46**, 10510 (2007).

[48] C. Clavaguéra-Sarrio, V. Vallet, D. Maynau, and C. J. Marsden, J. Chem. Phys. **121**, 5312 (2004).

[49] D. Majumdar, K. Balasubramanian, and H. Nitsche, Chem. Phys. Lett. **361**, 143 (2002).

[50] C. Angeli, R. Cimiraglia, S. Evangelisti, T. Leininger, and J.-P. Malrieu, J. Chem. Phys. **114**, 10252 (2001).

[51] C. Angeli, R. Cimiraglia, and J.-P. Malrieu, Chem. Phys. Lett. **350**, 297 (2001).

[52] C. Angeli, R. Cimiraglia, and J.-P. Malrieu, J. Chem. Phys. **117**, 9138 (2002).

[53] F. Neese, Wiley Interdiscip. Rev.: Comput. Mol. Sci. **2**, 73 (2012).

[54] A. Schäfer, C. Huber, and R. Ahlrichs, J. Chem. Phys. **100**, 5829 (1994).

[55] T. F. Miller, M. Eleftheriou, P. Pattnaik, A. Ndirango, D. Newns, and G. J. Martyna, J. Chem. Phys. **116**, 8649 (2002).

[56] I. T. Todorov, W. Smith, K. Trachenko, and M. T. Dove, J. Mater. Chem. **16**, 1911 (2006).

[57] J. K. Gibson, R. G. Haire, M. Santos, J. Marçalo, and A. de Matos, J. Phys. Chem. A **109**, 2768 (2005).

[58] Y. Marcus and A. Loewenschuss, J. Chem. Soc., Faraday Trans. **82**, 2873 (1986).

[59] L. V. Moskaleva, A. V. Matveev, S. Krüger, and N. Rösch, Chem. - Eur. J. **12**, 629 (2006).

[60] I.-C. Yeh and G. Hummer, J. Phys. Chem. B **108**, 15873 (2004).

[61] S. P. Tiwari, N. Rai, and E. J. Maginn, Phys. Chem. Chem. Phys. **16**, 8060 (2014).

[62] S. Kerisit and C. Liu, J. Phys. Chem. A **117**, 6421 (2013).

[63] M. Chopra and N. Choudhury, J. Phys. Chem. B **118**, 14373 (2014).

[64] J.-P. Simonin, I. Billard, H. Hendrawan, O. Bernard, K. Lützenkirchen, and L. Sémon, Phys. Chem. Chem. Phys. **5**, 520 (2003).

[65] G. Marx, R. Gauglitz, V. Friehmelt, and K. H. Feldner, J. Less-Common Met. **122**, 185 (1986).

[66] D. M. H. Kern and E. F. Orlemann, J. Am. Chem. Soc. **71**, 2102 (1949).

[67] J.-M. Andanson, M. Traïkia, and P. Husson, J. Chem. Thermodyn. **77**, 214 (2014).

[68] L. H. Jones and R. A. Penneman, J. Chem. Phys. **21**, 542 (1953).

[69] L. J. Basile, J. C. Sullivan, J. R. Ferraro, and P. LaBonville, Appl. Spectrosc. **28**, 142 (1974).

[70] P. Ball, Chem. Rev. **108**, 74 (2008).

[71] H. Ohtaki and T. Radnai, Chem. Rev. **93**, 1157 (1993).

[72] Y. Marcus, Chem. Rev. **88**, 1475 (1988).

[73] A. Melchior, J. M. Martínez, R. R. Pappalardo, and E. Sánchez Marcos, J. Chem. Theory Comput. **9**, 4562 (2013).

[74] M. L. San-Román, M. Carrillo-Tripp, H. Saint-Martin, J. Hernández-Cobos, and I. Ortega-Blake, Theor. Chem. Acc. **115**, 177 (2006).

[75] K. Morimoto, M. Kato, H. Uno, A. Hanari, T. Tamura, H. Sugata, T. Sunaoshi, and S. Kono, J. Phys. Chem. Solids **66**, 634 (2005).

[76] R. W. Impey, P. A. Madden, and I. R. McDonald, J. Phys. Chem. **87**, 5071 (1983).

[77] A. E. García and L. Stiller, J. Comput. Chem. **14**, 1396 (1993).

[78] E. I. Martín, J. M. Martínez, and E. Sánchez Marcos, J. Chem. Phys. **143**, 044502 (2015).